International Journal of Concrete Structures and Materials
Vol.10, No.2, pp.221–236, June 2016
DOI 10.1007/s40069-016-0144-9
ISSN 1976-0485 / eISSN 2234-1315

Mechanical Properties and Modeling of Amorphous Metallic Fiber-Reinforced Concrete in Compression

Ngoc-Hieu Dinh, Kyoung-Kyu Choi*, and Hee-Seung Kim

(Received December 30, 2015, Accepted April 26, 2016, Published online June 2, 2016)

Abstract: The aim of this paper is to investigate the compressive behavior and characteristics of amorphous metallic fiber-reinforced concrete (AMFRC). Compressive tests were carried out for two primary parameters: fiber volume fractions (V_f) of 0, 0.3, 0.6 and 0.8 %; and design compressive strengths of 27, 35, and 50 MPa at the age of 28 days. Test results indicated that the addition of amorphous metallic fibers in concrete mixture enhances the toughness, strain corresponding to peak stress, and Poisson's ratio at high stress level, while the compressive strength at the 28-th day is less affected and the modulus of elasticity is reduced. Based on the experimental results, prediction equations were proposed for the modulus of elasticity and strain at peak stress as functions of fiber volume fraction and concrete compressive strength. In addition, an analytical model representing the entire stress–strain relationship of AMFRC in compression was proposed and validated with test results for each concrete mix. The comparison showed that the proposed modeling approach can properly simulate the entire stress–strain relationship of AMFRC as well as the primary mechanical properties in compression including the modulus of elasticity and strain at peak stress.

Keywords: compressive strength, amorphous metallic fibers, fiber-reinforced concrete, Poisson's ratio, strain at peak stress, modulus of elasticity, stress–strain curve.

1. Introduction

For several decades, significant research has been performed to improve binder materials (cement, fly ash, and slag) and adhesives (superplasticizer, etc.) suitable for high performance construction materials (Constantinides et al. 2003; Jeong et al. 2015; Le et al. 2014; Sriravindrarajah et al. 2012; Divsholi et al. 2014; Sorensen et al. 2014). Based on the progress in concrete technology, high strength concrete (HSC) with compressive strength of 100 MPa or above has been developed and applied in various construction fields. Nonetheless, such HSC generally shows severe brittle behavior in compression compared to normal strength concrete (NSC) (Gettu et al. 1990; Wittmann 2002); HSC suddenly loses its load carrying capacity after reaching peak compressive strength. Partly due to the brittleness of HSC, ACI 318-14 (2014) limits the maximum value of $\sqrt{f_c'}$ to be 8.3 MPa in shear design of concrete structures. In addition, the ACI Manual of Concrete Practice (1998) limit the use of HSC in earthquake resisting structures.

For this reason, considerable research has been performed to improve the characteristics and the ductility of concrete (in particular HSC) in compression by the addition of fibers in concrete. In a study by Ezeldin and Balaguru (1992), the use of fibers in both NSC and HSC ranging from 35 to 85 MPa was found to increase toughness, compressive strength, strain corresponding to peak stress, and the secant modulus of elasticity. In addition, Ou et al. (2011) investigated the compressive stress–strain behavior of steel fiber-reinforced concrete (SFRC) with a high reinforcing index, which was defined as the product of fiber volume fraction and fiber aspect ratio. Their study indicated that the addition of hooked-end fibers to concrete matrix increases both material toughness and strain at the peak stress, while the modulus of elasticity and compressive strength of SFRC are less affected. Moreover, Chi et al. (2012) performed experiments to investigate the uniaxial compressive behavior of steel-polypropylene hybrid fiber-reinforced concrete (HFRC). It was observed that the compressive behavior of concrete can be improved by the addition of hybrid fibers and showed a variation according to fiber volume fractions of steel and polypropylene fibers and aspect ratio of steel fibers. Based on the test results, the optimum proportion of hybrid fibers was also investigated to achieve enhanced compressive strength and ductile compressive behavior. Recently, Srikar et al. (2016) investigated the residual compressive properties of polypropylene fiber- reinforced concrete exposed to high temperature by using digital image correlation method. It was reported that the polypropylene fibers improved the post-peak residual compressive strength and the toughness of concrete subjected to temperatures up to 300 °C. The stress–strain curves also show a significantly improvement in post peak behavior with increasing fiber volume fraction at all level of exposure temperatures.

Soongsil University, Seoul, Korea.
*Corresponding Author; E-mail: kkchoi@ssu.ac.kr

Recently, newly-developed fibers, known as amorphous metallic fibers (AMF), have been investigated by numerous researchers. Choi and Ku (2014) performed flexural tests on amorphous metallic fiber-reinforced concrete (AMFRC) and it was found that the addition of the fibers in concrete could significantly enhance flexural strength as well as toughness; a higher fiber volume fraction of up to 0.75 % could result in a more enhanced flexural behavior of concrete. Moreover, Hameed et al. (2010) and Won et al. (2012) demonstrated that the presence of amorphous metallic fibers increased the flexural toughness and strength and was more effective than the conventional steel fibers in terms of flexural toughness and strength. Additionally, Choi et al. (2014) investigated the shrinkage and corrosion resistance of amorphous metallic fiber-reinforce cement composites and conclude that amorphous metallic fibers displayed higher corrosion resistance than did steel in every degradation environment, and plastic shrinkage crack control performance was excellent. More recently, experiments performed by Choi et al. (2015) showed that the addition of AMF into concrete could significantly reduce the free drying shrinkage by 24 %; and in the restraint shrinkage tests (ring tests and slab tests), AMF delay crack development time as well as reduced crack width to 36.5–74.6 % according to the fiber volume fraction. Notwithstanding this, the mechanical properties of AMFRC in compression were not adequately investigated in the above studies.

In this current study, a compressive test on AMFRC was performed with variations of fiber volume fraction and concrete compressive strength. Based on the test results, primary compressive characteristics were investigated in terms of the modulus of elasticity, Poisson's ratio, strain corresponding to peak stress, and the toughness. In addition, an analytical model was proposed for simulating the entire compressive stress–strain curves of AMFRC as functions of the fiber volume fraction and concrete compressive strength.

2. Experimental Program

2.1 Materials

In order to investigate the influence of amorphous metallic fibers on the compressive behavior of concrete, three different concrete mix proportions were employed with the design compressive strengths of 27, 35 and 50 MPa at the 28-th day. The detailed proportions are presented in Table 1. The concrete matrix consisted of Type I Portland cement, natural river sand having a fineness modulus of 2.65, and crushed limestone with the maximum aggregate size of 13 mm and fineness modulus of 6.40. The grading of fine aggregate and coarse aggregate conformed to the requirement specified in ASTM C33 (2013). A super-plasticizer was used as an admixture with a dosage of cement content of 0.2–0.8 % to achieve adequate workability of fresh concrete in the presence of metallic fibers.

The fibers used in this test are a special type, called amorphous metallic fibers (AMFs). Figure 1 illustrates the configuration of AMFs. They are made of an amorphous alloy of the Fe family with a density of 7200 kg/m^3, straight ribbon type of 1.6 mm width, 30 mm length, 0.029 mm thickness (equivalent aspect ratio $L/d_f = 125$), modulus of elastic of 140 GPa, and yield tensile strength of 1700 MPa. Moreover, as shown in the scanning electron microscopy (SEM) image (Fig. 2), the amorphous metallic fibers also have a rough surface, which has been found to improve the bond strength between the fibers and the cementitious matrix (Choi et al. 2015). In this study, four different fiber volume fractions were employed: 0 % (control type), 0.3, 0.6, and 0.8 %. The dosages corresponding to the fiber volume fractions are 0, 21.6, 43.2, and 57.6 kg/m^3, respectively.

2.2 Mixing, Casting, and Curing Procedure

The concrete was mixed using a compulsive concrete mixer with a capacity of 0.6 m^3. First, the dry aggregate and cement were mixed for 1 min. Then, 80 % of water was added and mixing was continued for a further 1 min. The mixing was then continued with the fibers for 2 min. Finally, the remaining water along with the superplasticizer was poured gradually and mixing was continued for an additional 3 min.

The preparation procedure of specimens in this study follows ASTM C 192 (2015); the fresh concrete mix was cast in standard cylinders of 100 mm diameter and 200 mm height in three equal layers with each layer being rodded with 25 strokes using a tamping rod. For each batch, at least 5 specimens were cast and then covered with a wet cloth to prevent evaporation. After 24 h, they were demoulded and cured according to ASTM C31 (2015) in lime-saturated water at a temperature of 23 $\pm$ 1.7 °C before the loading test. As shown in Fig. 3, the water-heater was used to maintain the temperature in the container at 23 $\pm$ 1.7 °C due to the low temperature of the laboratory in winter.

2.3 Test Setup

The compressive test for cylindrical specimens was carried out according to ASTM C39 (2015). Before testing, the cylinders were flattened at both ends to ensure smooth surfaces to transfer the uniform load. The test was conducted using a hydraulically-powered machine with a capacity of 1000 kN. A data acquisition system was connected to the computer to record the load and strain data.

In this test, similar to a previous study (Xie et al. 2015), a compressometer was used with two high sensitive linear variable displacement transducers (LVDTs) on two opposite locations of the specimen as shown in Fig. 4. The strain was then calculated as the ratio between the average displacement of two LVDTs and the gauge length of 100 mm. To measure the transverse strain of the specimens, two concrete strain gauges with a length of 60 mm were attached horizontally at the mid height of the cylinder using a quick-curing adhesive, as illustrated in Fig. 5. In order to attach the strain gauges to the uneven and rough surfaces of the concrete specimens, the voids on the surfaces were filled with a suitable pre-coating material. To obtain the entire stress–

Table 1 Concrete mix proportions.

Design strength (MPa)	Design air content (%)	Design slump flow (mm)	W/C[a] (%)	S/a[b] (%)	Unit content (kg/m^3)					
					Water	Cement	Fine aggregate	Coarse aggregate	Admixture[c]	AMF[d] content
27	4.0 ± 1.0	150 ± 50	55	51.8	202	367	884	811	0.2	–
									0.4	21.6
									0.6	43.2
									0.8	57.6
35			45	43.8	216	480	695	880	0.2	–
									0.4	21.6
									0.6	43.2
									0.8	57.6
50			35	44.3	236	675	592	733	0.2	–
									0.4	21.6
									0.6	43.2
									0.8	57.6

[a] *W/C* water to cement ratio.
[b] *S/a* sand to aggregate ratio.
[c] Admixture in %.
[d] *AMF* amorphous metallic fiber.

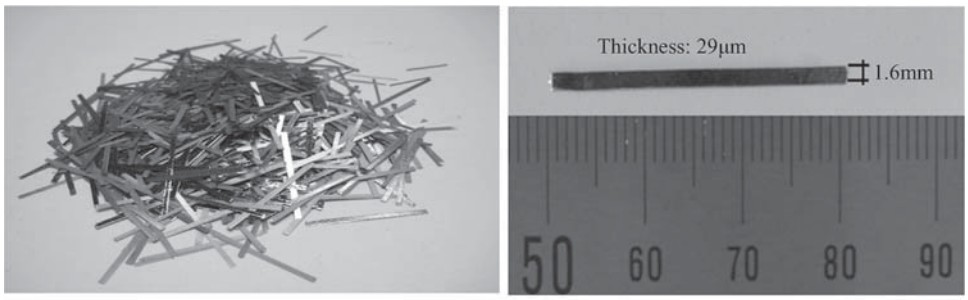

Fig. 1 Amorphous metallic fibers used in test.

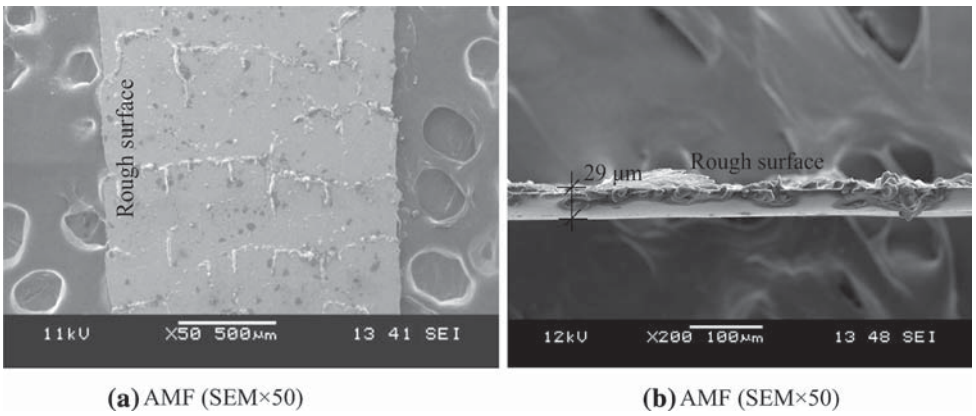

Fig. 2 Scanning electron microscopy photos of amorphous metallic fiber.

strain curve, a compression test was carried out using a displacement control method with a velocity of 0.005 mm/s according to a previous study (Chi et al. 2012). Both the displacement and strain data were collected using the data acquisition system. The test was intentionally ended at a vertical deformation of about 5 mm.

Fig. 3 Curing specimens following ASTM C31.

3. Experimental Results and Discussions

3.1 Properties of Fresh Concrete

The characteristics of fresh concrete using amorphous metal fibers were investigated based on an air content test and slump-flow test for each concrete mixture according to standards of ASTM C231 (2014) and ASTM C143 (2015).

The air content test results for different concrete mixes are given in Fig. 6. They indicate that the presence of amorphous metallic fibers in fresh concrete mix lead to a slight increase of air void content in the range of 0.4–0.6 %.

Figure 7 illustrates the relationship between fiber volume fraction and slump value according to different grades of concrete mix. It shows that a higher volume fraction of amorphous metallic fibers resulted in lower workability. In particular, for the fiber volume fraction of 0.8 % of 50 MPa concrete mix, the slump value obtained from experiment is 100 mm, which decreased by 47 % compared to plain fresh concrete mix (190 mm). To address this problem, further research is needed aiming to enhance the slump flow of fresh amorphous metal fiber-reinforced concrete mixture, by using high performance superplasticizer or optimum concrete mix proportion with the presence of fly ash and silica fume.

Fig. 4 Test setup for cylindrical specimens.

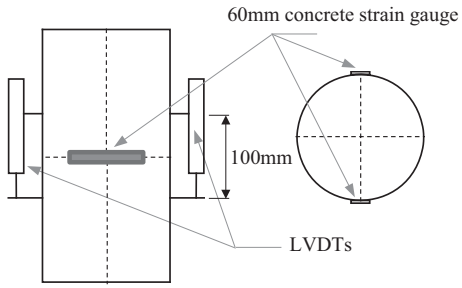

Fig. 5 Location of the strain gauge and LVDTs.

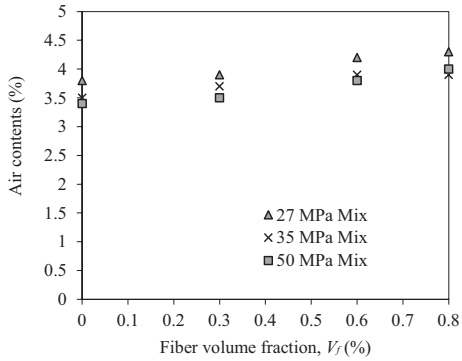

Fig. 6 Variation of air content according to fiber volume fraction.

3.2 Characteristics of Hardened Concrete

The important parameters characterizing the compressive behavior of plain and amorphous metal fiber-reinforced concrete were investigated and are summarized in the form of normalization in Table 2: compressive strength, the strain at peak stress, ultimate strain, elastic modulus, and toughness index.

3.2.1 Compressive Strength and Strain at Peak Stress

The strength test results are summarized in Table 2. In this table, the compressive strength of each test specimen

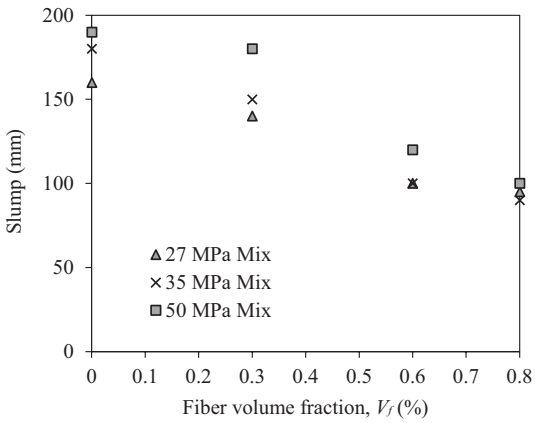

Fig. 7 Variation of slump according to fiber volume fraction.

Table 2 Summary of test results.

Type	Normalized compressive strength[a]	Normalized strain at peak stress[b]	Normalized elastic modulus[c]	Normalized Toughness index[d]	Normalized ultimate strain[e]
Plain 27	1.01	1.05	1.01	0.96	1.06
	0.99	0.92	1.01	1.14	0.79
	1.05	1.01	1.07	0.97	0.93
	0.97	1.02	0.97	0.95	1.23
	0.98	1.01	0.95	0.98	0.99
	$f_c = 28.69$ MPa	$\varepsilon_o = 2.40 \times 10^{-3}$	$E_c = 24.93$ GPa	$I = 2.21$	$\varepsilon_{ou} = 4.97 \times 10^{-3}$
AMF 27-03	0.95	0.99	0.94	1.01	0.89
	1.02	0.99	1.01	1.13	1.12
	1.08	1.04	1.10	1.23	1.15
	0.95	0.95	0.96	0.84	0.88
	1.00	1.03	1.00	0.79	0.97
	$f_c = 27.85$ MPa	$\varepsilon_o = 2.54 \times 10^{-3}$	$E_c = 23.33$ GPa	$I = 3.61$	$\varepsilon_{ou} = 7.82 \times 10^{-3}$
AMF 27-06	0.93	0.87	0.91	0.87	0.84
	1.01	1.02	1.03	1.11	1.13
	1.00	1.10	1.08	0.97	1.03
	1.00	0.98	0.98	1.01	0.98
	1.07	1.03	1.00	1.05	1.02
	$f_c = 28.17$ MPa	$\varepsilon_o = 2.80 \times 10^{-3}$	$E_c = 21.79$ GPa	$I = 4.30$	$\varepsilon_{ou} = 8.30 \times 10^{-3}$
AMF 27-08	0.97	1.00	0.98	0.99	1.12
	1.00	1.00	1.01	0.93	0.96
	0.98	0.96	0.97	1.03	1.03
	1.04	1.06	1.05	1.10	0.95
	1.01	0.98	1.00	0.96	0.94
	$f_c = 28.64$ MPa	$\varepsilon_o = 3.02 \times 10^{-3}$	$E_c = 18.94$ GPa	$I = 4.52$	$\varepsilon_{ou} = 9.58 \times 10^{-3}$
Plain 35	1.03	0.98	1.02	0.94	0.98
	1.01	1.03	1.01	1.05	1.02
	0.97	0.97	0.97	0.97	1.02
	1.05	1.08	1.03	0.98	1.08
	0.95	0.93	0.97	1.06	0.90
	$f_c = 39.27$ MPa	$\varepsilon_o = 2.49 \times 10^{-3}$	$E_c = 28.44$ GPa	$I = 2.43$	$\varepsilon_{ou} = 4.50 \times 10^{-3}$
AMF 35-03	0.99	0.99	0.96	1.07	0.94
	0.99	1.00	0.99	0.99	1.03
	0.96	0.97	1.05	0.96	1.04
	1.03	1.01	1.02	1.05	1.03
	1.02	1.02	0.98	0.93	0.96
	$f_c = 39.92$ MPa	$\varepsilon_o = 2.62 \times 10^{-3}$	$E_c = 27.20$ GPa	$I = 3.97$	$\varepsilon_{ou} = 6.65 \times 10^{-3}$
AMF 35-06	0.96	0.95	1.02	1.02	0.94
	0.99	0.99	1.05	1.03	1.01
	1.02	1.02	0.99	0.98	1.01
	1.03	1.05	1.00	1.01	1.03
	1.00	0.99	0.95	0.95	1.01
	$f_c = 41.46$ MPa	$\varepsilon_o = 2.85 \times 10^{-3}$	$E_c = 25.31$ GPa	$I = 4.25$	$\varepsilon_{ou} = 7.86 \times 10^{-3}$

Table 2 continued

Type	Normalized compressive strength[a]	Normalized strain at peak stress[b]	Normalized elastic modulus[c]	Normalized Toughness index[d]	Normalized ultimate strain[e]
AMF 35-08	1.03	1.01	1.02	0.93	1.00
	0.92	0.94	0.92	1.01	0.98
	1.03	1.04	1.03	1.01	1.06
	1.00	1.03	0.99	1.01	1.00
	1.03	0.98	1.03	1.04	0.96
	$f_c = 39.88$ MPa	$\varepsilon_o = 3.22 \times 10^{-3}$	$E_c = 23.58$ GPa	$I = 4.49$	$\varepsilon_{ou} = 9.91 \times 10^{-3}$
Plain 50	1.00[f]	0.98[f]	1.00[f]	0.82[f]	0.64[f]
	1.13	1.10	1.10	0.96	1.09
	1.08	1.04	1.02	1.06	1.07
	0.95	0.95	0.95	0.97	0.96
	0.84	0.91	0.93	1.01	0.88
	$f_c = 52.31$ MPa	$\varepsilon_o = 2.59 \times 10^{-3}$	$E_c = 31.11$ GPa	$I = 2.20$	$\varepsilon_{ou} = 4.33 \times 10^{-3}$
AMF 50-03	1.03	0.99	1.02	1.05	1.01
	1.14	1.15	1.06	0.79	0.95
	1.00	0.98	1.01	0.97	0.93
	0.86	0.93	0.92	1.08	1.02
	0.97	0.96	0.99	1.11	1.08
	$f_c = 51.02$ MPa	$\varepsilon_o = 2.65 \times 10^{-3}$	$E_c = 29.21$ GPa	$I = 4.18$	$\varepsilon_{ou} = 6.56 \times 10^{-3}$
AMF 50-06	0.94	0.92	0.94	0.99	0.92
	1.03	1.09	1.07	1.03	1.15
	1.02	1.00	0.99	0.98	0.94
	1.03	1.04	1.00	1.01	1.05
	0.99	0.95	1.00	1.00	0.95
	$f_c = 51.56$ MPa	$\varepsilon_o = 2.87 \times 10^{-3}$	$E_c = 26.89$ GPa	$I = 4.31$	$\varepsilon_{ou} = 7.86 \times 10^{-3}$
AMF 50-08	1.07	0.99	1.14	1.03	0.90
	1.02	0.92	1.03	0.94	0.92
	0.99	1.02	0.94	1.00	1.05
	0.93	1.08	0.89	1.00	1.14
	1.00	0.99	1.00	1.04	1.00
	$f_c = 49.86$ MPa	$\varepsilon_o = 3.34 \times 10^{-3}$	$E_c = 25.07$ GPa	$I = 4.52$	$\varepsilon_{ou} = 10.00 \times 10^{-3}$

[a] It is normalized by the average compressive strength, f_c.
[b] It is normalized by the average strain at the peak stress, ε_o.
[c] It is normalized by the average elastic modulus, E_c.
[d] It is normalized by the average toughness index, I.
[e] It is normalized by the average ultimate strain, ε_{ou}.
[f] Neglected data because the instability of descending branch after peak stress.

normalized by the average value for each concrete mix are reported. The measured average compressive strengths of plain concrete at the 28-th day were 28.69, 39.27, and 52.30 MPa, while the design strengths were 27, 35, and 50 MPa.

Figure 8 presents the typical stress–strain curve of AMFRC with the design strength of 27 MPa. In general, amorphous metallic fibers do not affect the compressive strength of concrete. The difference in compressive strength between the amorphous metal fiber-reinforced concrete and plain concrete is within 0.17–2.93 % (see Table 2), which is negligible. According to previous studies (ACI Manual of Concrete Practice 1998; Neves and Gonµalves 2000), the fibers transfer stress across the micro cracks even in the compressive test, which could lead to higher compressive strength. However, the fibers could cause some disturbance

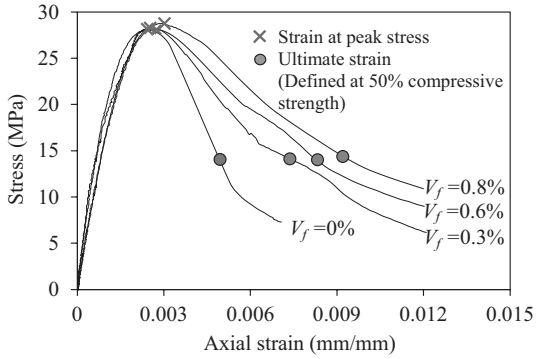

Fig. 8 Typical stress–strain curve of 27 MPa concrete compressive strength for different fiber volume fractions.

in the concrete matrix, which results in more voids in the concrete micro structure (Neves and Gonμalves 2000) and has a negative effect on compressive strength. Due to the trade-off between micro-crack bridging and additional voids, the influence of amorphous metal fibers on compressive strength is not significant.

In Figs. 8 and 9, the compressive strain, ε_{of}, corresponding to the peak stress of AMFRC is presented. ε_{of} shows an increasing trend with increasing fiber volume fraction, V_f, and this trend is consistent for all specimens, regardless of concrete compressive strength. For example, at 0.8 % fiber volume fraction, ε_{of} is almost 0.00291–0.00362, which is almost 130 % that (0.0022–0.00286) of plain concrete. Figures 8 and 10 present the ultimate compressive strain, ε_{ou}, corresponding to the stress at which concrete is crushed. The value of ε_{ou} is computed at limited stress $\sigma_u = 0.5\, f_c$ in the descending branch of the stress–strain curve according to the CEB-FIP Model Code (1990). It also shows an increase of ultimate strain accompanying the increase of fiber volume fraction, V_f. This phenomenon is consistent even in the case of higher compressive strength specimens of 50 MPa, which is normally considered to be brittle. This demonstrates that the addition of amorphous metallic fibers assists in efficiently controlling the propagation of micro-cracks into macro-cracks during the post-peak stage of concrete. For HSC with the compressive strength of 70–100 MPa, additional future tests need to be conducted to verify the effect of amorphous metallic fibers on the ultimate compressive strain of HSC.

3.2.2 Failure Modes

The typical failure modes of AMFRC specimens observed under uniaxial compressive test in this study are illustrated in Fig. 11 (Cunha et al. 2006). Vertical cracks were formed immediately before reaching peak stress, and inclined shear failure cracks were formed at the beginning of the softening phase. This process lasted until each specimen had completely failed. The vertical cracks and the crack opening can be explained by fracture mode I, while the inclined shear crack causing crack opening and sliding can be explained by the combination of fracture modes I and II (Cunha et al. 2006).

Figure 12 illustrates the typical crack patterns of 50 MPa-specimens for different fiber volume fractions. It is evident that the presence of fibers modified the crack patterns of the concrete cylindrical specimens, whereby the plain specimen was governed by a few macro cracks. However, the AMFRC specimen showed many vertical or diagonal cracks with a

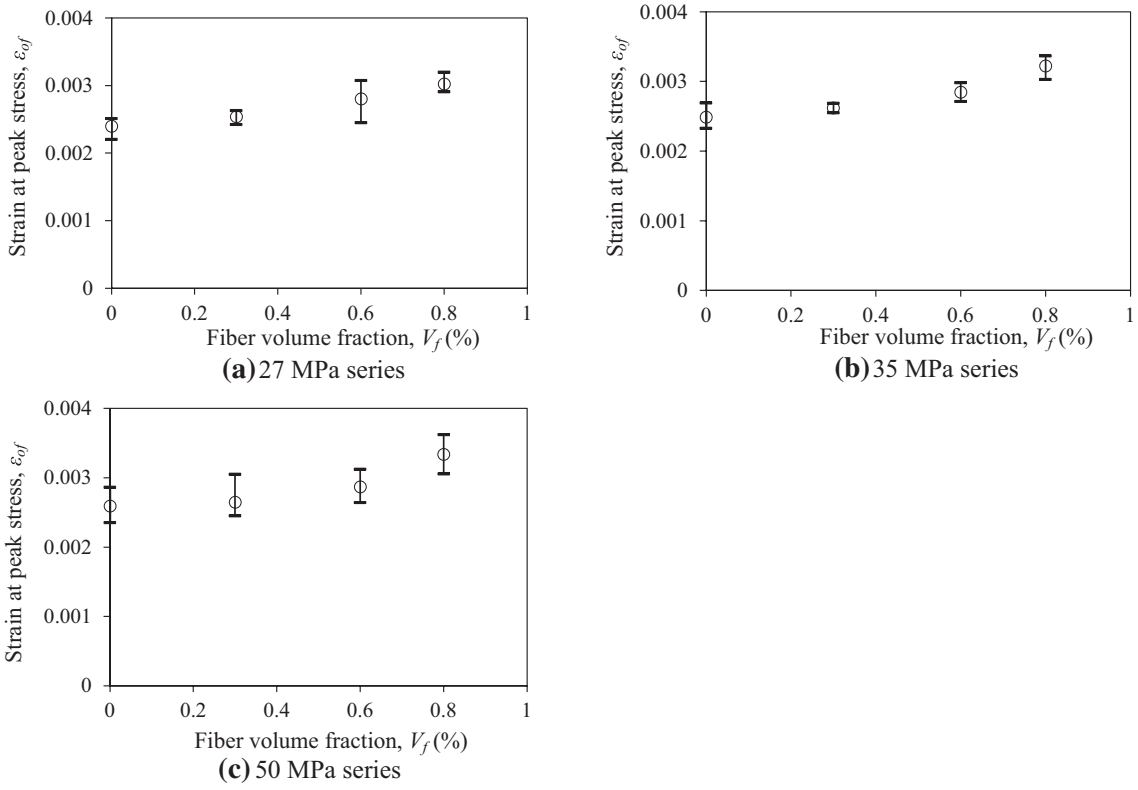

Fig. 9 Variation of ε_{of} of AMFRC for different fiber volume fractions and concrete compressive strengths.

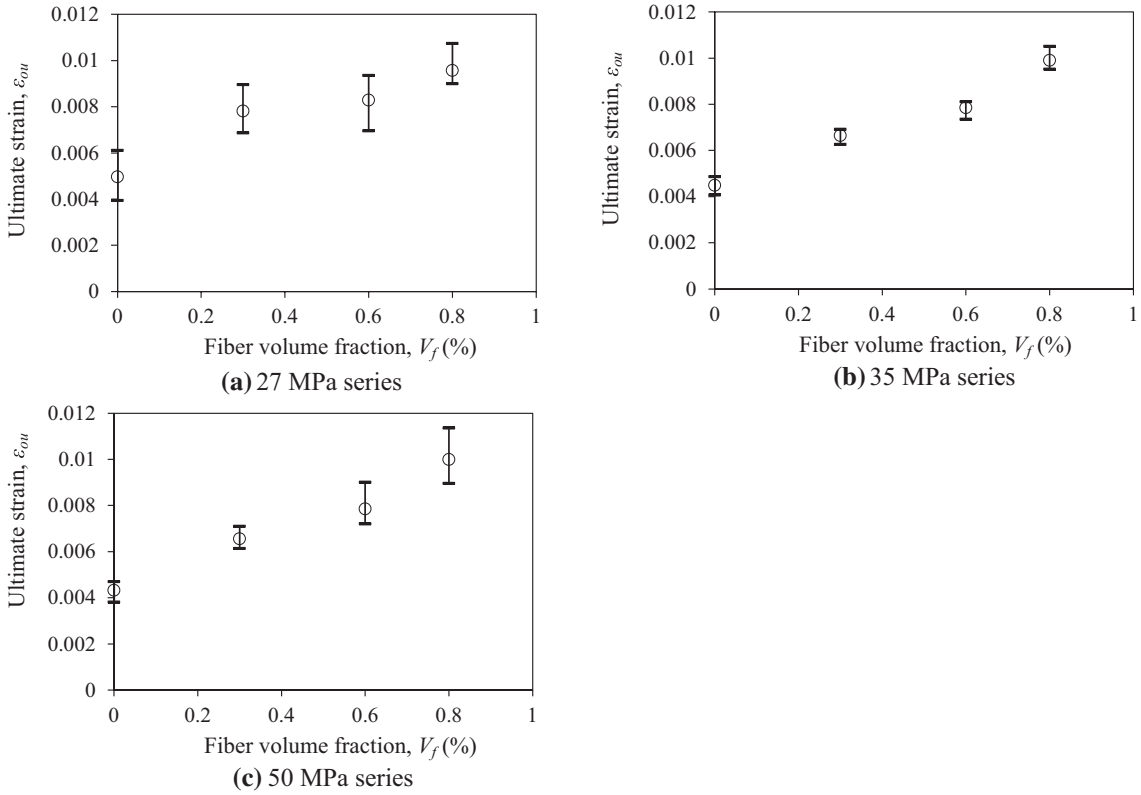

Fig. 10 Variation of compressive ultimate strain, ε_{ou}, of AMFRC for different fiber volume fractions and concrete compressive strengths.

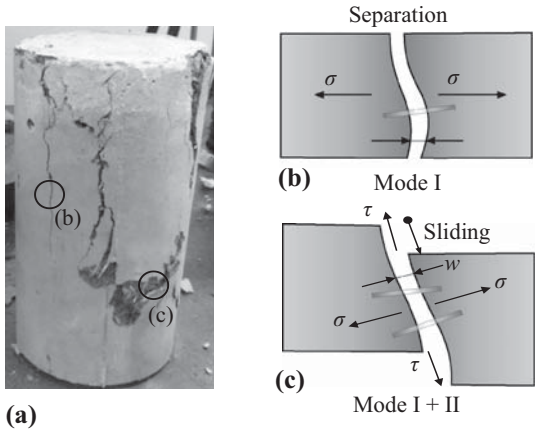

Fig. 11 Failure mechanism of AMFRC under compression (Cunha et al. 2006).

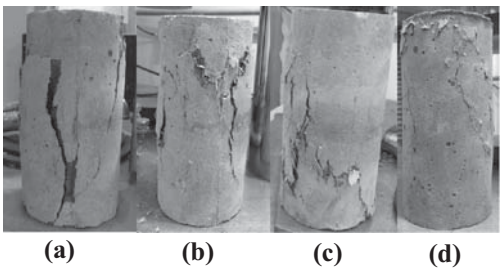

Fig. 12 Crack patterns of specimens with different fiber volume fractions (V_f) after failure: **a** $V_f = 0$ %; **b** $V_f = 0.3$ %; **c** $V_f = 0.6$ %; and **d** $V_f = 0.8$ %.

narrow crack width, and in particular, the specimen with 0.8 % fiber volume fraction did not show significant concrete spalling and macro cracks even after failure. This phenomenon is partly due to the bridging mechanism of fibers during the post-cracking stage of specimens (ACI Manual of Concrete Practice 1998).

3.2.3 Modulus of Elasticity

The value of elastic modulus of concrete in compression was obtained from the stress–strain curve of each specimen based on the method according to ASTM C469 (2014):

$$E_c = (S_2 - S_1)/(\varepsilon_2 - 0.00005) \quad (1)$$

where E_c = modulus of elasticity (MPa), S_2 = stress corresponding to 40 % of ultimate load (MPa), S_1 = stress corresponding to a longitudinal strain, ε_1, of 0.00005 (MPa), and ε_2 = longitudinal strain produced by stress S_2.

Figure 13 presented the influence of fiber volume fraction on modulus of elasticity in the case of concrete compressive strength of 35 MPa. In addition, the calculated results for each specimen in the form of normalization and the mean value for the different concrete mix are reported in Table 2. Based on this, the correlation between the fiber volume fraction and elastic modulus for various compressive strengths is presented in Fig. 14. Similar to a previous study on steel fiber-reinforced concrete (Ou et al. 2011), the presence of amorphous fibers in the concrete matrix also causes a decrease in the modulus of elasticity. In particular, for the fiber volume fraction of 0.8 %, the elastic modulus

was reduced by 24.03, 17.09, 19.47 % in the case of 27, 35 and 50 MPa concrete, respectively. This is because the fibers parallel to the load direction act as voids in the concrete matrix (Rossi and Harrouche 1990; Mansur et al. 1999).

3.2.4 Toughness Index

Toughness is one of the important parameters explaining the ductility of the compressive behavior of concrete after reaching peak stress. The toughness is defined as the area under the stress–strain curve. To quantify the effect of fiber on the toughness of concrete in compression, Fanella and Naaman (1985) proposed the toughness index (TI) while Ezeldin and Balaguru (1992) proposed another approach using the toughness ratio (TR), which is the ratio of toughness of fiber-reinforced concrete to that of a rigid plastic material. In this study, the toughness is measured using a toughness index, which is defined as the ratio of area under the stress–strain curve at a strain of 0.015 and the area at peak stress, as show in Fig. 15. The value of 0.015 has also been used in Nataraja et al. (1999) and Bhargava et al. (2006). Based on the above definition using the strain of 0.015, in the present study, the toughness index obtained from each specimen and the average value are presented in Table 2.

Figure 16 shows the influences of amorphous fiber volume fraction on the toughness index according to the concrete compressive strength. In plain concrete, the value of the toughness index varies between 2.12 and 2.43 for the three different compressive strengths. In the 0.8 % fiber volume fraction, the toughness index reaches almost 4.5, which is about two times that of plain concrete. It is

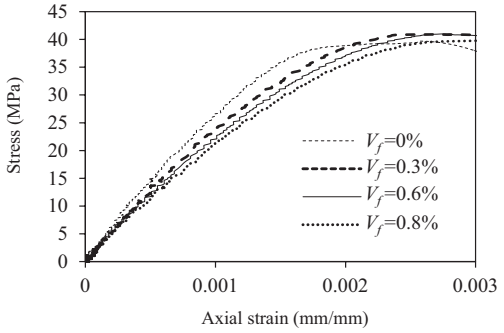

Fig. 13 Typical stress–strain relationship (35 MPa series).

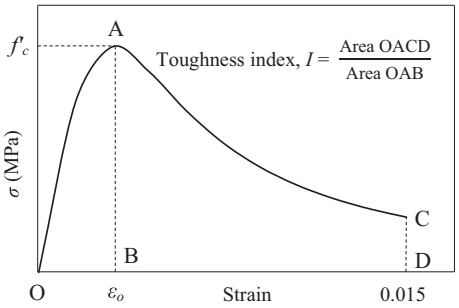

Fig. 15 Definition of compressive toughness index (I).

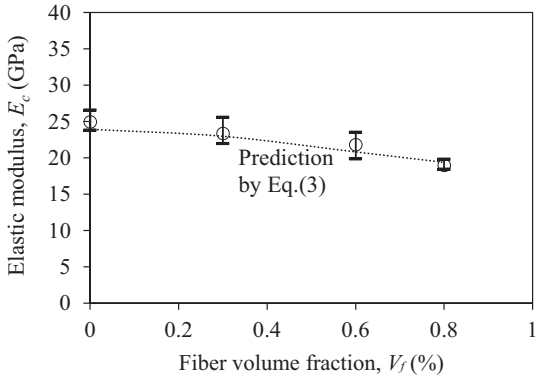

(a) 27 MPa series

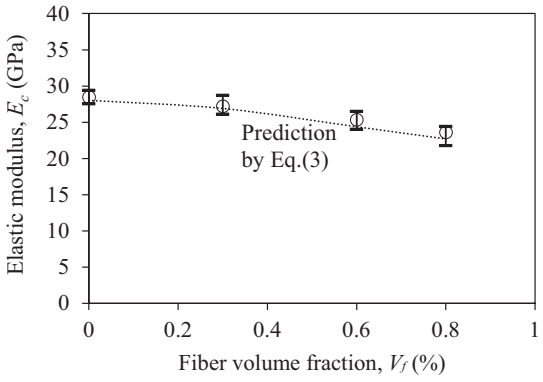

(b) 35 MPa series

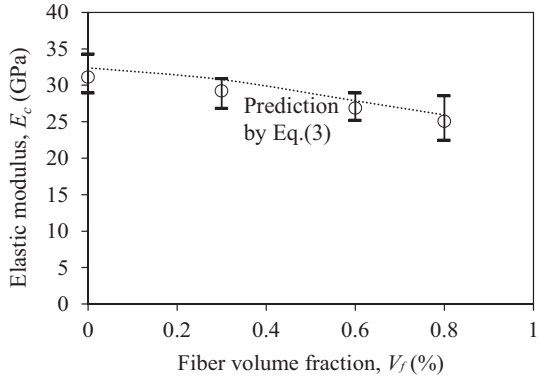

(c) 50 MPa series

Fig. 14 Variation of elastic modulus of AMFRC for different fiber volume fractions and concrete compressive strengths.

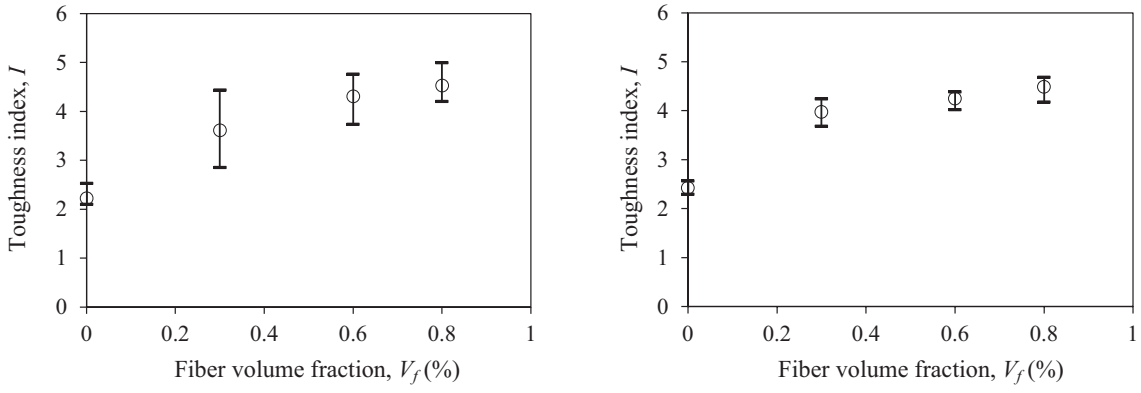

(a) 27 MPa series **(b)** 35 MPa series

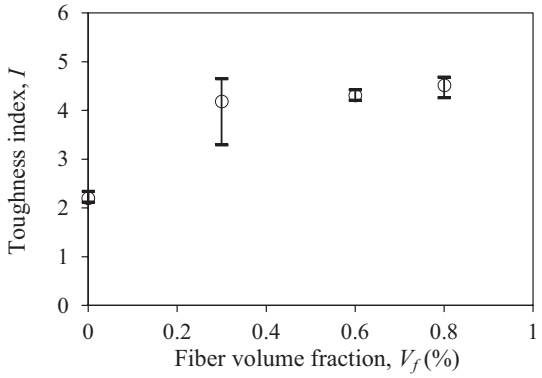

(c) 50 MPa series

Fig. 16 Effects of fiber volume fraction on compressive toughness index.

interesting that the toughness index also shows almost the same increasing trend even in higher strength concrete of 50 MPa, which is usually expected to be brittle. This proves that the presence of amorphous metallic fibers in concrete enhances the post failure behavior in compression.

3.2.5 Poisson's Ratio

In terms of Poisson's ratio (υ_c), which is the ratio of transverse to axial strain, Fig. 17 shows the typical variation in Poisson's ratio according to the normalized stress of different concrete compressive strengths. It can be observed that in case of 27 MPa, below the normalized stress level of 40 %, Poisson's ratio shows almost constant value of 0.2; however, after stress level of 60 %, the Poisson's ratio of the plain specimen tends to increase suddenly, leading to a stretch in the curve. In the case of 35 and 50 MPa concrete, Poisson's ratio shows almost constant value of 0.2 below 60 % stress level and a sharp increase after 80 % stress level for plain specimen. This result was expected because the external layer is damaged more quickly than the core of the specimen (Ferretti et al. 1999). On the other hand, in the case of amorphous fiber-reinforced specimens, the increased fiber

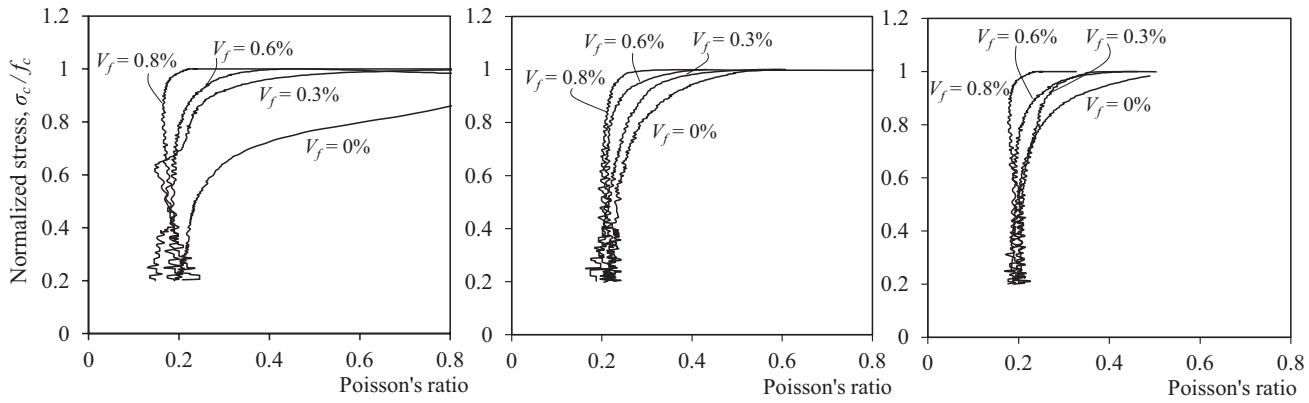

(a) 27 MPa series **(b)** 35 MPa series **(c)** 50 MPa series

Fig. 17 Normalized stress-Poisson's ratio relationship for different concrete compressive strengths.

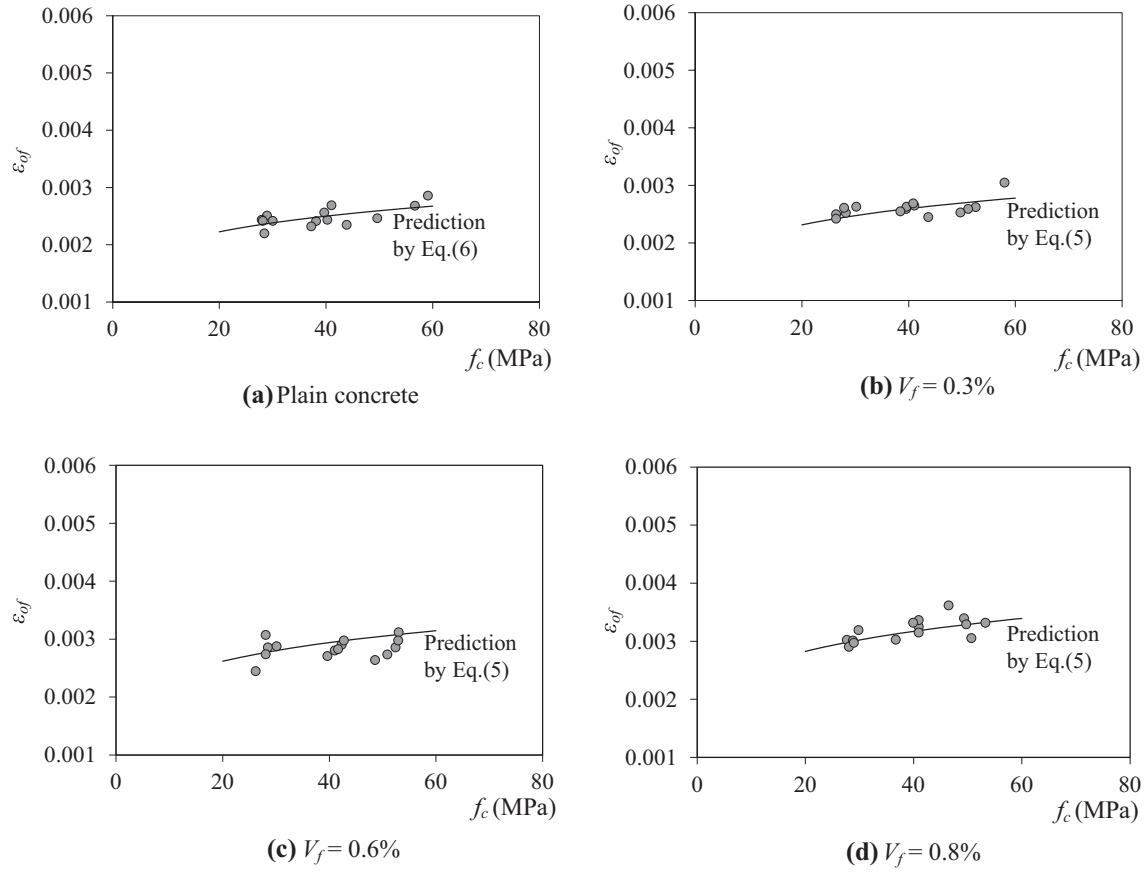

(a) Plain concrete

(b) $V_f = 0.3\%$

(c) $V_f = 0.6\%$

(d) $V_f = 0.8\%$

Fig. 18 Variation of compressive strain at peak stress according to compressive strength and fiber volume fraction.

content in the concrete matrix induces less stretch in the normalized stress—Poisson's ratio curves. Interestingly, in the case of the fiber volume fraction of 0.8 %, the Poisson's ratio of 0.2 is maintained as constant until the peak stress level. This phenomenon can be observed for all cases of 0.8 % fiber volume fraction of different the concrete compressive strengths (27, 35, and 50 MPa). It was demonstrated that the presence of amorphous metal fibers in a concrete matrix has limited expansion in the horizontal direction, resulting in less destructive external surface and contributing to the stabilization of Poisson's ratio at high stress level.

4. Modeling and its Validation of Compressive Characteristics of AMFRC

4.1 Modulus of Elasticity

Mansur et al. (1999) proposed an analytical equation to evaluate the elastic modulus considering the fiber volume fraction and compressive strength as

$$E_f = (A - B\,V_f)\sqrt[3]{f_c} \tag{2}$$

where E_c is in GPa, V_f is in percentage, and f_c is in MPa.

In this study, based on the regression analysis, the elastic modulus, E_{cf}, of amorphous metallic fiber-reinforced concrete was defined as a function of the elastic modulus, E_c, of plain concrete and fiber volume fraction, $V_f(\%)$

$$E_{cf} = E_c(1.04 - 0.3V_f) \tag{3}$$

For the limited test data obtained in this study, the best fitting equation for E_c was defined as

$$E_c = 4480\sqrt{f_c}\ (MPa) \tag{4}$$

Figure 14 compares the prediction obtained from Eq. (3) and the test results. The figure shows a relatively good correlation between the experimental data and the predicted results. However, since the value of the elastic modulus of concrete strongly depends on the nature of coarse aggregate (Baalbaki et al. 1991; Aïtcin and Mehta 1990; Gutierrez and Canovas 1995), for different aggregate types, the above equation needs to be adjusted.

4.2 Strain at Peak Stress

In the test results observed in this study, it was found that the strain, ε_{of}, at the peak stress of the amorphous metallic fiber-reinforced concrete was strongly related to the strain at the peak stress of plain concrete and fiber volume fraction. Based on regression analyses for each group of tested specimens, an analytical equation to evaluate the strain at peak stress was proposed as

$$\varepsilon_{of} = \varepsilon_o(0.9 + 0.46\,V_f) \tag{5}$$

where V_f = fiber volume fraction (%) and ε_o = strain corresponding to peak stress of plain concrete, determined from the regression analysis of the experiment data. For the

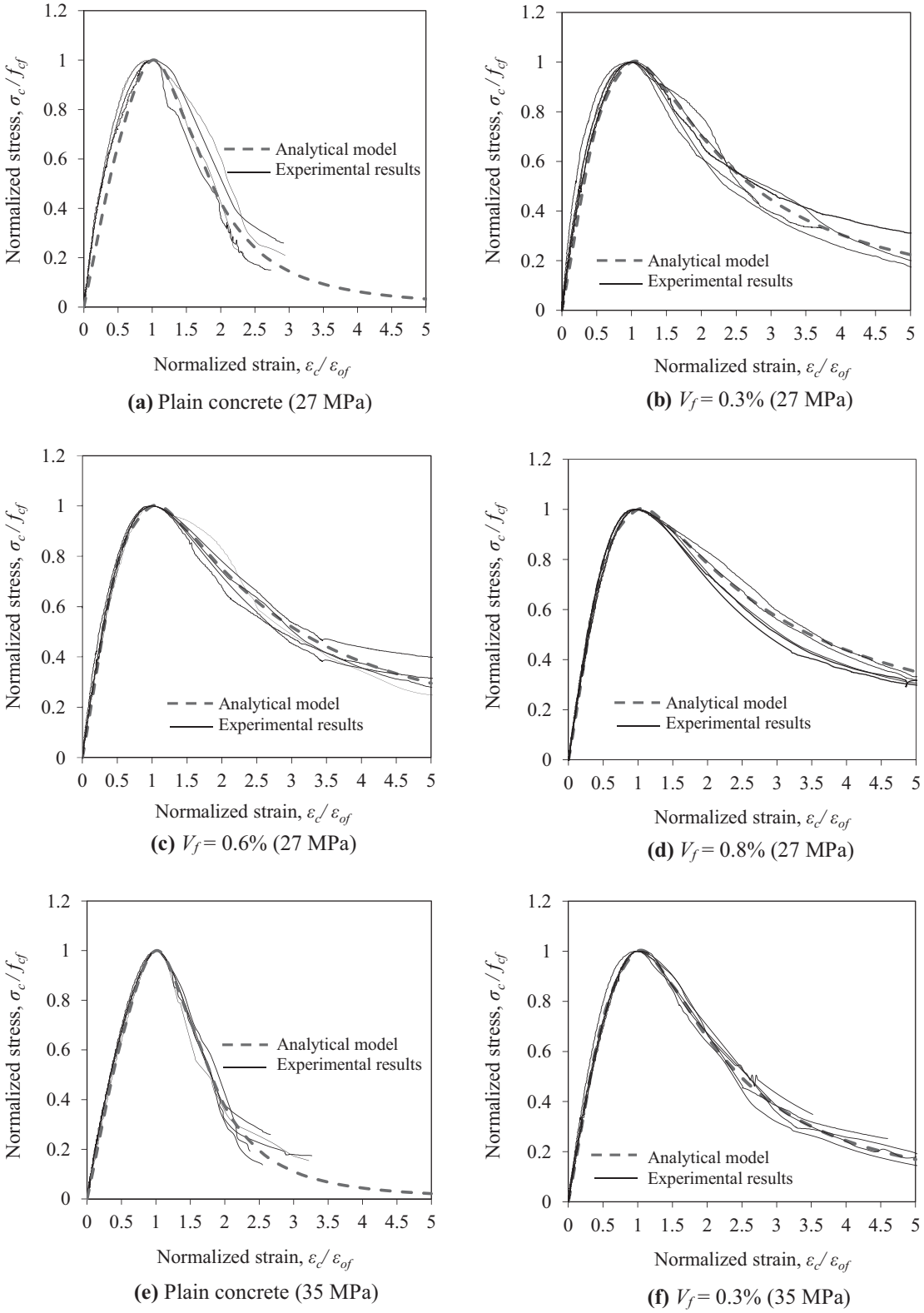

(a) Plain concrete (27 MPa)
(b) V_f = 0.3% (27 MPa)
(c) V_f = 0.6% (27 MPa)
(d) V_f = 0.8% (27 MPa)
(e) Plain concrete (35 MPa)
(f) V_f = 0.3% (35 MPa)

Fig. 19 Verification of proposed model for stress–strain relationship.

limited test data obtained in this study, the best fitting equation for ε_o was defined as

$$\varepsilon_o = \frac{6.05 f_c^{0.667}}{E_c} \tag{6}$$

In Eq. (6), E_c is the modulus of elasticity of plain concrete Eq. (4).

The predicted values of the compressive strain at peak stress of plain concrete and amorphous metal fiber-reinforced concrete from Eqs. (5) and (6) are compared with the experimental data in Fig. 18. Generally, the model shows a good prediction of the strain at peak stress according to compressive strength and fiber volume fraction.

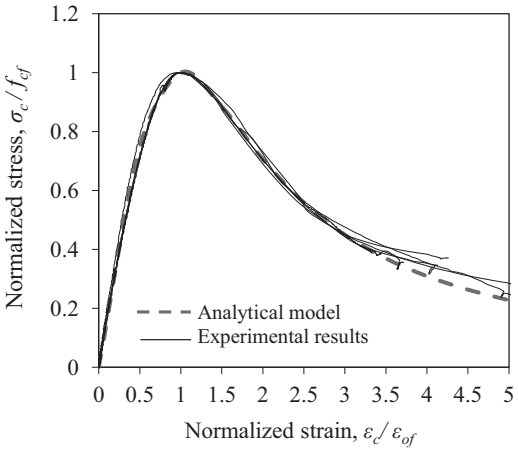

(g) V_f = 0.6% (35 MPa)

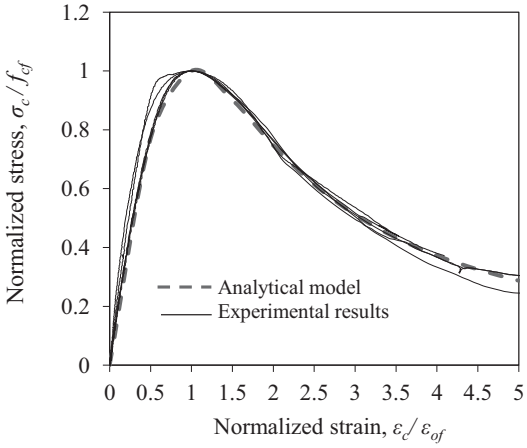

(h) V_f = 0.8% (35 MPa)

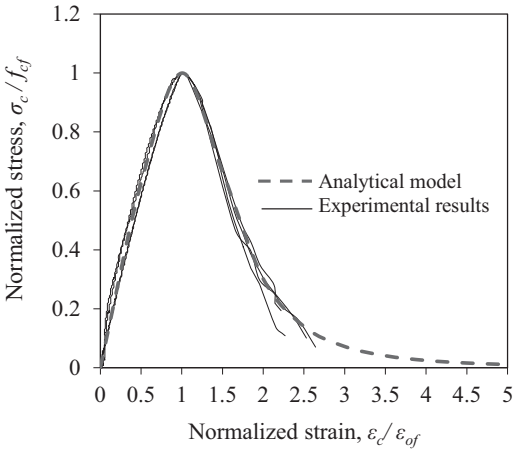

(i) Plain concrete (50 MPa)

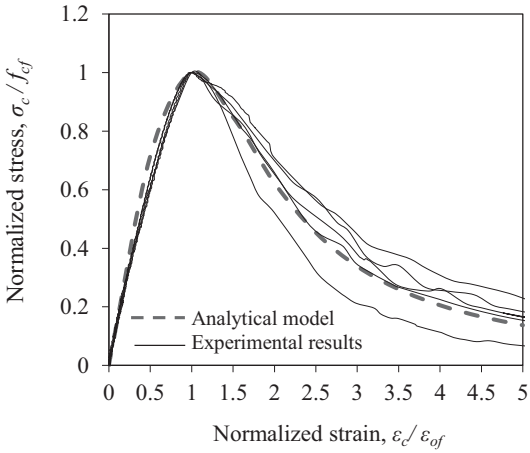

(j) V_f = 0.3% (50 MPa)

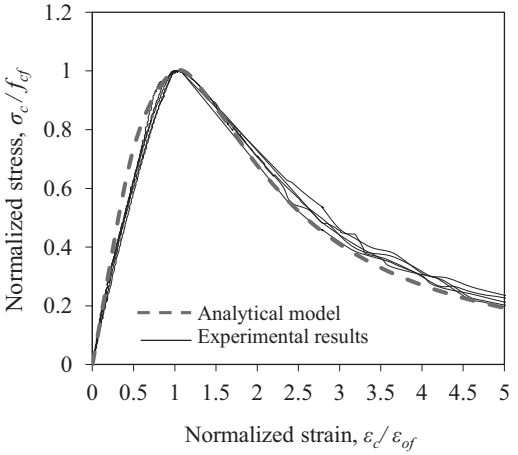

(k) V_f = 0.6% (50 MPa)

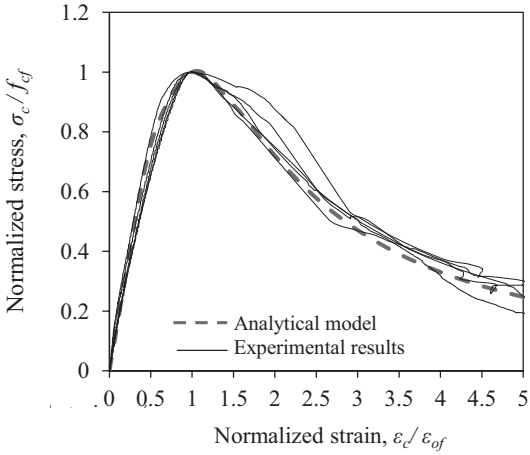

(l) V_f = 0.8% (50 MPa)

Fig. 19 continued

4.3 Stress–Strain Relationship

To date, many analytical models have been developed to represent the stress–strain curve for plain concrete under uniaxial compression. Among the models, the expression proposed by Carreira and Chu (1985) was used as a basis in this study to obtain the stress–strain relationship for both plain concrete and AMFRC. The model was also used in Ezeldin and Balaguru (1992), Mansur et al. (1999), Nataraja et al. (1999), and Araújo (2002).

In this study, the model by Carreira and Chu (1985) was modified to consider the fiber effects as

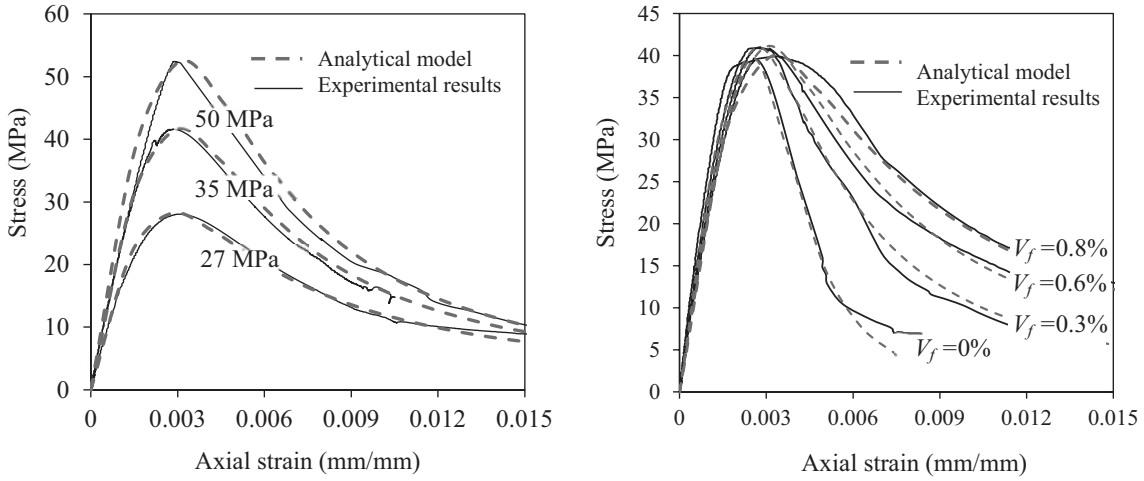

(a) $V_f = 0.6\%$ **(b)** 35 MPa series

Fig. 20 Comparison of proposed model for stress–strain relationship with different compressive strength and different fiber volume fraction.

$$\frac{\sigma_c}{f_{cf}} = \frac{\beta \frac{\varepsilon_c}{\varepsilon_{of}}}{\beta - 1 + \left(\frac{\varepsilon_c}{\varepsilon_{of}}\right)^{\beta}} \tag{7}$$

where f_{cf} is the compressive strength of plain or AMFRC, ε_{of} is the strain corresponding to compressive strength of the materials used; σ_c and ε_c are the stress and strain on the curve, respectively; and β is a material parameter representing the influence of fibers in the descending branch of the stress–strain curve. It is noticed that the smaller value of β produces a less steep descending branch in the stress–strain curve. For a given value of compressive strength, ε_{of} is determined using Eqs. (5) and (6), and thus the only variable is β.

Based on multi-linear regression analysis, the β value was defined as functions of fiber volume fraction, V_f(%), and the compressive strength of plain concrete, f_c (MPa)

$$\beta = \begin{cases} \sqrt[4]{f_c}(1.71 - 2.14\,V_f) & \text{for} \quad 0 \le V_f < 0.3 \\ \sqrt[4]{f_c}(1.184 - 0.355\,V_f) & \text{for} \quad V_f \ge 0.3 \end{cases} \tag{8}$$

Figure 19 compares the compressive stress–strain curves obtained in the test results and those predicted by the proposed model. Due to the variation in compressive strength and strain at peak stress of different specimens, the stress–strain relationships were compared in a normalized manner. Figures 20a and 20b illustrate typical stress–strain curves from experimental results and proposed analytical model in the cases of 0.6 % amorphous metallic fiber volume fraction and concrete compressive strength of 35 MPa, respectively. The figures showed that the proposed model properly predicted the test results throughout all the curves. Thus, the proposed model is expected to be used for structural analysis of AMFRC for different compressive strengths and fiber volume fractions.

5. Conclusions

In this paper, the characteristics of amorphous metallic fiber-reinforced concrete in fresh and hardened stages were investigated. The following conclusions can be drawn from the experimental results:

- The addition of amorphous metallic fibers to concrete reduces the workability according to fiber volume fraction and increases the air contents of fresh concrete mixture in a range of 0.4–0.6 %.
- Generally, amorphous metallic fibers don't affect the compressive strength of concrete, the difference in compressive strength between the amorphous metal fiber-reinforced concrete and plain concrete is only 0.17–2.93 %. However, strain corresponding to peak stress, ultimate strain and toughness in compression were found to be increased proportionally to the fiber dosage in the concrete mix.
- The elastic modulus shows a decreasing tendency with increasing fiber volume fraction.
- The existing of amorphous metallic fibers in concrete matrix reduces the expansion of concrete in the horizontal direction, which contributes to the stabilization of Poisson's ratio in high stress level.
- Equations to predict the modulus of elasticity and the strain at peak stress of amorphous metal fiber-reinforced concrete were proposed as functions of fiber volume fraction and the concrete compressive strength, and were validated by the test results. The prediction by the equations showed a good correlation with the test data.
- A stress–strain curve is also proposed to represent the complete stress–strain relationship based on multi-linear regression analysis method. The proposed modeling approach was found to present a good correlation with the experimental results.

However, the application of the proposed model is limited to the test condition of this study: the maximum aggregate size of 13 mm and fiber length of 30 mm. Thus, further investigation and validation are necessary for different test conditions.

Acknowledgments

This research was supported by the National Research Foundation of Korea Grant funded by the Korean Government (NRF-2014R1A1A2053499).

References

ACI 318-14 (2014). *Building code requirements for structural concrete*.

Aïtcin, P. C., & Mehta, P. K. (1990). Effect of coarse aggregate characteristics on mechanical properties of high-strength concrete. *ACI Materials Journal, 87*(2), 103–107.

American Concrete Institution. State-of-the-Art Report on Fiber Reinforced Concrete. *ACI Manual of Concrete Practice* 1998, Part 5. Farmington Hills, MI: ACI International

Araújo, DL. (2002). Cisalhamento entre viga e laje pré-moldadas ligadas mediante nichos preenchidos com concreto de alto desempenho, *Tese de D.Sc*., Universidade de São Paulo, Escola de Engenharia de São Carlos, Brasil

ASTM International (2013). *ASTM C33/C33M*: *standard specification for concrete aggregates*.

ASTM International (2014). *ASTM C231/C231M: standard test method for air content of freshly mixed concrete by the pressure method.*

ASTM International (2014). *ASTM C469/C469 M: standard test method for static modulus of elasticity and poisson's ratio of concrete in compression*.

ASTM International (2015). *ASTM C192/C192M: standard practice for making and curing concrete test specimens in the laboratory.*

ASTM International (2015). *ASTM C31/C31M*: *standard practice for making and curing concrete test specimens in the field*.

ASTM International (2015). *ASTM C39/C39M*: *standard test method for compressive strength of cylindrical concrete specimens*.

ASTM International (2015). *ASTM C143/C143M: standard test method for slump of hydraulic cement concrete.*

Baalbaki, W., Benmokrane, B., Chaallal, O., & Aitcin, P. C. (1991). Influence of coarse aggregate on elastic properties of high-performance concrete. *ACI Materials Journal, 88*(5), 499–503.

Bhargava, P., Sharma, U. K., & Kaushik, S. K. (2006). Compressive stress-strain behavior of small scale steel fibre reinforced high strength concrete cylinders. *Journal of advanced concrete technology, 4*(1), 109–121.

Carreira, D. J., & Chu, K. H. (1985, November). Stress-strain relationship for plain concrete in compression. In *ACI Journal proceedings* (Vol. 82, No. 6). ACI.

CEB-FIP Model Code (1990). *Design code*.

Chi, Y., Xu, L., & Zhang, Y. (2012). Experimental Study on Hybrid Fiber-Reinforced Concrete Subjected to Uniaxial Compression. *Journal of Materials in Civil Engineering, 26*(2), 211–218.

Choi, H. (2010). Shrinkage cracking characteristics of micro steel fiber-reinforced concrete. *Master Thesis*; Soongsil University, Seoul, Korea.

Choi, S. J., Hong, B. T., Lee, S. J., & Won, J. P. (2014). Shrinkage and corrosion resistance of amorphous metallic-fiber-reinforced cement composites. *Composite Structures, 107*, 537–543.

Choi, K. K., & Ku, D. O. (2014). Flexural behaviour of amorphous metal-fibre-reinforced concrete. *Proceedings of the ICE-Structures and Buildings, 168*(1), 15–25.

Choi, K. K., Truong, G. T., & Choi, S. J. (2015). Restrained shrinkage cracking of amorphous metallic fibre-reinforced concrete. *Proceedings of the ICE-Structures and Buildings, 168*(12), 902–914.

Constantinides, G., Ulm, F. J., & Van Vliet, K. (2003). On the use of nanoindentation for cementitious materials. *Materials and Structures, 36*(3), 191–196.

Cunha, V. M., Barros, J. A., & Sena-Cruz, J. M. (2006). Compression behaviour of steel fibre reinforced self-compacting concrete–age influence and modeling (p. 49). *Report 06-DEC/E-04*, University of Minho.

Divsholi, B. S., Lim, T. Y. D., & Teng, S. (2014). Durability properties and microstructure of ground granulated blast furnace slag cement concrete. *International Journal of Concrete Structures and Materials, 8*(2), 157–164.

Ezeldin, A. S., & Balaguru, P. N. (1992). Normal-and High-Strength Fiber-Reinforced Concrete under Compression. *Journal of materials in civil engineering*.

Fanella, D. A., & Naaman, A. E. (1985, July). Stress-strain properties of fiber reinforced mortar in compression. In *ACI Journal proceedings* (Vol. 82, No. 4). ACI.

Ferretti, E., Viola, E., Di Leo, A., Pascale, G. (1999). Crack propagation and macroscopic behaviour of concrete in compression. *XIV Congresso nazionale AIMETA*, Como, 6–9 (in Italian).

Gettu, R., Bazant, Z. P., & Karr, M. E. (1990). Fracture properties and brittleness of high-strength concrete. *ACI Materials Journal, 87*(6), 608–618.

Gutierrez, P. A., & Canovas, M. F. (1995). The modulus of elasticity of high performance concrete. *Materials and Structures, 28*(10), 559–568.

Hameed, R., Turatsinze, A., Duprat, F., & Sellier, A. (2010). Study on the flexural properties of metallic-hybrid-fiber-reinforced concrete. *Maejo International Journal of Science and Technology, 4*(2), 169–184.

Jeong, Y., Park, H., Jun, Y., Jeong, J. H., & Oh, J. E. (2015). Microstructural verification of the strength performance of ternary blended cement systems with high volumes of fly ash and GGBFS. *Construction and Building Materials, 95*, 96–107.

Le, H. T., Nguyen, S. T., & Ludwig, H. M. (2014). A study on high performance fine-grained concrete containing rice husk ash. *International Journal of Concrete Structures and Materials, 8*(4), 301–307.

Mansur, M. A., Chin, M. S., & Wee, T. H. (1999). Stress-strain relationship of high-strength fiber concrete in compression. *Journal of Materials in Civil Engineering, 11*(1), 21–29.

Naaman, A. E., Wight, J. K., & Abdou, H. (1987). SIFCON connections for seismic resistant frames. *Concrete International, 9*(11), 34–39.

Nataraja, M. C., Dhang, N., & Gupta, A. P. (1999). Stress–strain curves for steel-fiber reinforced concrete under compression. *Cement & Concrete Composites, 21*(5), 383–390.

Neves, R., & Gonμalves, A. (2000). *Steel fibre reinforced conerete-durability related properties*. Lisbon, Portugal: LNEC. (in Portuguese).

Ou, Y. C., Tsai, M. S., Liu, K. Y., & Chang, K. C. (2011). Compressive behavior of steel-fiber-reinforced concrete with a high reinforcing index. *Journal of Materials in Civil Engineering, 24*(2), 207–215.

Rossi, P., & Harrouche, N. (1990). Mix design and mechanical behaviour of some steel-fibre-reinforced concretes used in reinforced concrete structures. *Materials and Structures, 23*(4), 256–266.

Sorensen, C., Berge, E., & Nikolaisen, E. B. (2014). Investigation of fiber distribution in concrete batches discharged from ready-mix truck. *International Journal of Concrete Structures and Materials, 8*(4), 279–287.

Srikar, G., Anand, G. A. A. & Suriya Prakash, S. (2016). A study on residual compression behavior of structural fiber reinforced concrete exposed to moderate temperature using digital image correlation. *International Journal of Concrete Structures and Materials* (Published online: 19 February 2016*).*

Sriravindrarajah, R., Wang, N. D. H., & Ervin, L. J. W. (2012). Mix Design for Pervious Recycled Aggregate Concrete. *International Journal of Concrete Structures and Materials, 6*(4), 239–246.

Wittmann, F. H. (2002). Crack formation and fracture energy of normal and high strength concrete. *Sadhana, 27*(4), 413–423.

Won, J. P., Hong, B. T., Choi, T. J., Lee, S. J., & Kang, J. W. (2012). Flexural behaviour of amorphous micro-steel fibre-reinforced cement composites. *Composite Structures, 94*(4), 1443–1449.

Xie, J. H., Guo, Y. C., Liu, L. S., & Xie, Z. H. (2015). Compressive and flexural behaviours of a new steel-fibre-reinforced recycled aggregate concrete with crumb rubber. *Construction and Building Materials, 79*, 263–272.